coatings

MDPI

Article

Electrodeposition Based Preparation of Zn–Ni Alloy and Zn–Ni–WC Nano-Composite Coatings for Corrosion-Resistant Applications

Channagiri Mohankumar Praveen Kumar [1], Avinash Lakshmikanthan [2], Manjunath Patel Gowdru Chandrashekarappa [3,*], Danil Yurievich Pimenov [4] and Khaled Giasin [5]

1 Department of Chemistry, PES Institute of Technology and Management, Visvesvaraya Technological University, Belagavi 590018, India; praveen.cm@pestrust.edu.in
2 Department of Mechanical Engineering, Nitte Meenakshi Institute of Technology, Visvesvaraya Technological University, Belagavi 590018, India; avinash.laks01@gmail.com
3 Department of Mechanical Engineering, PES Institute of Technology and Management, Visvesvaraya Technological University, Belagavi 590018, India
4 Department of Automated Mechanical Engineering, South Ural State University, Lenin Prosp. 76, 454080 Chelyabinsk, Russia; danil_u@rambler.ru
5 School of Mechanical and Design Engineering, University of Portsmouth, Portsmouth PO1 3DJ, UK; Khaled.giasin@port.ac.uk
* Correspondence: manju09mpm05@gmail.com; Tel.: +91-9844859032

Citation: Kumar, C.M.P.; Lakshmikanthan, A.; Chandrashekarappa, M.P.G.; Pimenov, D.Y.; Giasin, K. Electrodeposition Based Preparation of Zn–Ni Alloy and Zn–Ni–WC Nano-Composite Coatings for Corrosion-Resistant Applications. *Coatings* **2021**, *11*, 712. https://doi.org/10.3390/coatings11060712

Academic Editors: Edoardo Proverbio and Ludmila B. Boinovich

Received: 28 April 2021
Accepted: 11 June 2021
Published: 13 June 2021

Abstract: Zinc (Zn) is one of the five most widely consumed metals in the world. Indeed, more than 50% of all the zinc produced is used in zinc-galvanizing processes to protect steel from corrosion. Zn-based coatings have the potential for use as a corrosion-resistant barrier, but their wider use is restricted due to the poor mechanical properties of Zn that are needed to protect steel and other metals from rusting. The addition of other alloying elements such as Ni (Nickle) and WC (Tungsten Carbide) to Zn coating can improve its performance. This study investigates, the corrosion performance of Zn–Ni coating and Zn–Ni–WC composite nanocoatings fabricated on mild steel substrate in an environmentally friendly bath solution. The influence of WC nanoparticles on Zn–Ni deposition was also investigated. The surface morphologies, texture coefficients via XRD (X-ray diffraction), SEM (Scanning Electron Microscopy), and EDS (Energy-dispersive X-ray spectroscopy) were analyzed. The electrochemical test such as polarization curves (PC) and electrochemical impedance spectroscopy (EIS) resulted in a corrosion rate of 0.6948 Å/min for Zn–Ni–WC composite nanocoating, and 1.192 Å/min for Zn–Ni coating. The results showed that the Zn–Ni–WC composite nanocoating reduced the corrosion rate by 41.71% and showed an 8.56% increase in microhardness compared to the hardness of the Zn–Ni coating. These results are augmented to better wettable characteristics of zinc, which developed good interfacial metallurgical adhesion amongst the Ni and WC elements. The results of the novel Zn–Ni–WC nanocomposite coatings achieved a great improvement of mechanical property and corrosion protection to the steel substrate surface.

Keywords: Zn–Ni alloy; Zn–Ni–WC composite; nanocoatings; hardness; corrosion; electrodeposition

1. Introduction

The processing of different grades of steel alloys has a noticeable, commercial application due to their low cost and excellent mechanical and tribological properties [1]. Each steel grade often has its characteristics (phases, precipitates, properties) that are useful for certain applications [2]. The poor corrosion resistance of steel alloys limits their use in the construction industry [3], orthopedic implants [4], boat structures [5], manufacturing [6], and nuclear power plant [7] parts. According to the World Corrosion Organization, the annual cost of corrosion worldwide is estimated to exceed $1.8 trillion (in 2009) and $2.25 trillion (in 2019), which accounts for 3–4% of the annual world GDP of industrialized

countries [8,9]. The functional steel parts failure due to corrosion results in increased annual world steel production for compensation [10]. Therefore, immediate attention is required to study the appropriate methods that can enhance the corrosion resistance of steel alloys and improve their service life.

The galvanizing method is a widely accepted industry practice to protect steel substrate from corrosion [11]. The addition of alloying elements tends to increase the corrosion resistance of copper and nickel-based superalloys [12,13]. For high-temperature-sensitive engineering applications, there exists a lack of stability in the base or parent material, which inhibits their use as alloy processing route for corrosion-resistant methods [8,14]. The use of advanced coating techniques ensures the deposition of a wide range of metallic and non-metallic materials for different applications [15]. Coating techniques alter the surface properties (i.e., improve anti-corrosive and anti-wear resistance) of substrate material and ensure satisfactory function for prolonged service life subjected to a specific working environment [16,17]. The adhesion between coating-substrate is treated as the major contributing factor to obtaining reliable performance in engineered parts [18]. The deposited coating must be strong enough to sustain and transfer the applied loads to the coating–substrate interface, thereby proper functioning of the coating–substrate adhesion must ensure strong interfacial bonding requirements [19]. Coating–substrate adhesion quality is primarily dependent on the selection of appropriate coating methods. Numerous coating techniques are developed for surface protection of substrate or matrix material such as physical (sol-gel, cold spray, warm spray, physical vapor deposition), chemical (chemical vapor deposition), electrochemical (micro-arc oxidation, electrodeposition), laser cladding, and thermal (arc-wire spray, high-velocity oxy-fuel coating, plasma spray) methods [20,21]. Each coating method possesses their advantages and inherent limitations, and the selection of appropriate coating methods are of economic and industrial relevance [17,20]. Electrochemical deposition methods (electrochemical deposition, anodic oxidation, galvanic cell reactions, and polymerization reactions) are simpler, quicker, and highly repeatable; control the growth of kinetics of coating deposits; and offer larger coating surface areas with desired morphologies [22]. The electrodeposition technique is a single-step process which does not require expensive materials, equipment, and processing methods (i.e., tedious chemical treatment) for coating deposits on substrate material [22–24]. Therefore, significant attention must be paid to the application of different coating materials. The electrodeposition technique protects metallic surfaces from electrochemical deterioration, which is of industrial and economic relevance.

In recent years, the application of electrodeposition process-based metals/alloys and composite coatings on substrate materials resulted in excellent properties [25]. The choice of coating materials from a wide range of potential materials (e.g., organic: monomeric and polymeric; inorganic: metals, dielectric, metal oxides, and halides) to protect the substrate surface from corrosion and wear resistance is often treated as a tedious task for manufacturers [26–28]. Organic coatings are cost-effective but are often limited in their extensive use due to their poor wear resistance and hardness [29]. The excellent properties (i.e., hardness, strength, corrosion, and wear resistance) of metallic coatings are due to excellent adhesive characteristics among the coating substrate [30]. The wide classification of coating materials and techniques led to difficulties in selecting metallic materials (aluminum, titanium, chromium, molybdenum, cobalt, platinum, yttrium, zirconium) for enhanced corrosion and wear resistance without hindering the mechanical, thermal, and chemical properties [20]. Zinc served as a sacrificial protective coating material for steel in many engineering applications [31]. Zinc-based coatings possess excellent chemical stability, which protects pump compressor pipes, concrete sewer pipes, and wastewater pipes from bio-corrosion [32,33]. Cadmium coatings can be highly toxic and carcinogenic when deposited onto steel. Therefore, they were replaced by zinc-based coatings at a low cost with enhanced corrosion resistance, weldability, and ductile characteristics [34–37].

Zinc offers better wettable characteristics that could help to enhance the interfacial (coating–substrate material) bonding characteristics and thus resulting in higher mechanical

strength, anti-corrosion, and tribological properties [38–40]. Zinc possesses better wettable characteristics and therefore the use of hard materials (e.g., carbides: silicon carbide and tungsten carbide; oxides: iron oxide, zirconium dioxide, aluminum oxide, titanium dioxide, and silicon dioxide) as secondary phase materials in composite coatings results in excellent hardness, corrosion resistance, wear resistance, and high-temperature oxidation resistance for many industrial components [41–45]. Therefore, the study of zinc-based electrodeposited multi-layer composite nanocoatings ensures better coating properties at low costs, which are useful for industrial applications. Zn protects the steel substrate from corrosion, but their high consumption rates limit their wider applications [46]. Therefore, Zn coatings with major alloying elements such as nickel, cobalt, chromium, and iron could enhance the corrosion resistance characteristics [47].

Zn–Ni alloy coatings are composed of zinc (85%) and nickel (15%) and are commonly electroplated on carbon steel as a protective coating [48]. Zn–Ni alloy coatings are highly resistant to thermal loads and therefore are applied on bolts, threaded parts, brake systems, and fuel system components [45]. The use of multi-layer and composite coatings widens their applications (e.g., automotive, electrical transmission, fluid transfer, aerospace, and defense) due to their enhanced properties [45]. Multi-layered zinc-based alloy coatings (Zn–Co, Zn–Ni, Zn–Ni-Co, Zn–Al_2O_3–Cr_2O_3, Zn–TiO_2–WO_3, Zn–WO_3, Zn–Fe–Mo) are applied with the electrodeposition technique to evaluate the corrosion resistance characteristics [41,42,47,49–51]. The presence of Fe_2O_3, Al_2O_3, TiO_2, ZrO_2, SiO_2, and Co particles in the Zn–Ni bath solution results in better corrosion resistance [44–46]. The hardness of the coatings is not investigated in their research efforts [44]. The composite coatings Zn–Ni–Co and Zn–Ni–Fe_2O_3 resulted in enhanced corrosion resistance than the Zn–Ni alloy coatings [44,46]. Zinc-based antifouling environmentally friendly coatings are potential substitute material to copper, not only for creating better artificial surfaces for corrosion inhibition on ship and submarine parts, but also for their low toxicity to aquatic organisms [52]. Zinc-based silicon carbide nanocomposite coatings based on the electrodeposition technique resulted in refined grain size compared to galvanostatic coatings [53]. The addition of iron in zinc composite coatings enhances the mechanical strength at the rate of compromised ductility, cost, and corrosion rate for load-bearing applications [54]. Tungsten carbide (WC) material finds major applications in many engineering fields (e.g., the manufacture of cutting tools, machines, mining parts, catalysts, and so on) [55]. Tungsten carbide (WC) nanoparticles improve the interfacial metallurgical bonding that strengthens the Zn–Fe and nickel-based composite coatings with enhanced corrosion and wear resistance, microstructure, and ductility [54,56–58]. Tungsten carbide nanoparticles improve the thermal stability (phase and anti-oxidation) of copper composed of a 40% zinc alloy [59]. Zinc is proven to be a bioabsorbable material and their compromising poor mechanical properties have limited their wide use in pediatric applications [60]. Tungsten carbide (WC) particles reinforced to zinc composite coatings improve their inherent mechanical bonding strengths [60]. Nickel and tungsten carbide particles were previously used to prepare coatings used for biomedical applications [54,60–62]. It was confirmed from the above literature review that, the novel biocompatible Zn–Ni alloy and Zn–Ni–WC nanocomposites coatings are ideally best suited for a wide range of surface engineering applications.

Significant research efforts are made to protect steel substrate with a wide range of alloy/composite coatings. However, limited work is available in the open literature on developing Zn–Ni–WC composite nanocoatings and their characterizations (e.g., microhardness and corrosion rate) to protect the steel substrate used in various industrial applications. In addition, electrodeposition based on low-cost coating techniques possessing precise control over thickness and thus reduced material waste that can offer complex profiled parts are not studied yet on zinc–nickel alloys and Zn–Ni–WC composites coating samples. The Ni metallic particles [61,62] and the WC nanoparticles (known for their biocompatibility) [54,60] are incorporated into the Zn coatings in a bath solution (10% diluted H_2SO_4 + 90% diluted $NaHCO_3$), which are potentially stable and are not yet discussed in

the open literature. In the present work, electrodeposited coatings (Zn–Ni alloy and Zn–Ni–WC: WC concentration of 1 g/L) were developed on the steel substrate and were examined with electrochemical tests (PC and EIS), followed by validation with non-electrochemical tests (XRD, SEM). The impact of Ni metallic particles and WC nanoparticles on the hardness and corrosion resistance of the Zinc composite coatings was discussed. The obtained microhardness and corrosion rate results are compared with published literature and their practical usefulness was validated.

2. Materials and Methods

2.1. Materials and Electrodeposition Method

The electrodeposition of the Zn–Ni alloy and the Zn–Ni–WC composites nanocoatings were applied on the substrate, i.e., mild steel possessing a geometry of 50 mm × 40 mm × 1 mm, from a sulphate bath. The details of the bath solution prepared with analytical-grade chemicals and Millipore water are presented in Table 1.

Table 1. Electrolytic solution composition.

Constituents of Zn–Ni Bath Solution in (g/L)	Experimental Parameters
$NiSO_4$—60	pH—3.0
Na_2SO_4—40	Anode—Zn metal
H_3BO_3—24	Cathode—Mild steel
$ZnSO_4$—240	Current density—4 A/dm^2
SDS (Sodium Dodecyl Sulphate)—2	Stirring rate—300 rpm
WC—1.0	Cathode dimension—50 mm × 40 mm × 1 mm
-	Plating time—20 min

The equal surface area of pure zinc (nickel ions were present in bath solution) and mild steel plates are used as anode and cathode, respectively. The mild steel plates were mechanically polished with different grades of emery paper until they obtained a smooth and uniform surface. The specimens were then degreased in vapors of trichloroethylene and immersed in 10% HCl to remove dust and rust (if any was present). The plates were then washed with water, followed by air-drying, and then immersed in a plating bath solution. The bath solution was maintained at pH 3, using 10% H_2SO_4 and $NaHCO_3$. Before the electroplating, the composite coating bath solution was agitated for about 24 h using a magnetic stirrer at 600 rpm. Then, it was subjected to ultrasonification for about 30 min. The temperature during agitation and vibration was maintained equal to 25 ± 5 °C, and the potential of hydrogen (pH) is 3.0. The current density for plating was kept fixed to 4 A/dm^2. The deposition was carried out using a regulated DC power source, under the stagnant condition of the bath solution. Figure 1 describes the electrodeposition technique employed to develop the nanocomposites discussed in detail in the authors' earlier studies [44,63].

2.2. Microstructural Characterization

The morphologies of Zn–Ni alloy and Zn–Ni–WC composite coating were examined through SEM (JEOL-JEM-1200-EX II, Tokyo, Japan). Chemical elements and the nanoparticles dispersed in the coated electrodeposits were analyzed via SEM with EDS. The average crystallite size of coatings in electrodeposits (Zn–Ni, Zn–Ni–WC) was subjected to XRD analysis (Philips PW 3710 XRD, Amelo, The Netherland) with copper Kα radiation (set at 30 mA and 40 kV)). Methods such as Williamson–Hall plot, Le Bail, Warren–Averbach, and Scherrer's models can be applied to determine the crystal size of the coating deposits [64–66]. In the present work, the Scherrer equation (Equation (1)) was applied to estimate the average crystallite size of electrodeposits based on the XRD data patterns (i.e., peak width at mean height) [51,63,64].

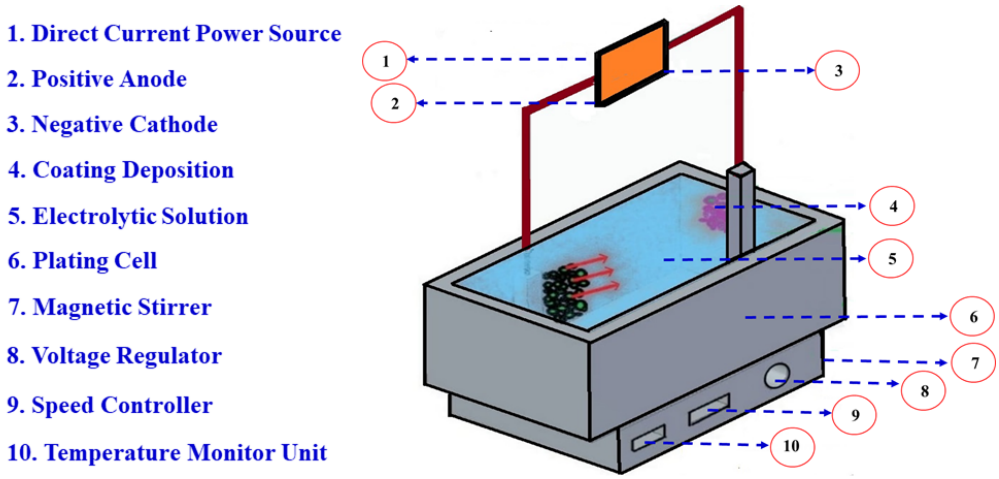

Figure 1. Electrodeposition technique set up used to develop the nanocomposites.

$$L_{hkl} = \frac{0.9\lambda}{\beta \cos\theta} \quad (1)$$

Here, L_{hkl} is the median particle size, λ represents the x-ray tube wavelength, β depicts the spacing of the peak, and θ is the Braggs angle.

The coating thickness has been calculated based on the equations derived from the practical experiments by Parthasarathy [67]. Equation (2) was used to estimate the coating thickness as follows:

$$T = \frac{m}{A \times d} \quad (2)$$

where m is the mass of deposit, A is the cross-sectional area in cm^2, and the density of coating material is in g/cm^3

2.3. Microhardness Measurement

The microhardness of electrodeposited composite coating specimens were examined as per ASTM E92-82 test standards using Vickers's microhardness tester (Clemex digital microhardness tester, Japan). The hardness measurements are carried out on the coating samples (possessing a coating thickness of ≈20 µm) subjected to a load of 50 g for 10 s dwell time. Experiments are repeated thrice on each coating condition to reduce experimental variations and an average of 15 microhardness indentations (five measurements on each sample with three replicates) measured at many spatial locations on the coated samples was considered.

2.4. Corrosion Rate Measurements

The coating (Zn–Ni alloy, Zn–Ni–WC composite) samples were examined to estimate corrosion rate, with the help of Potentiodynamic polarization and EIS via CHI660C electrochemical workstation comprising of a three-electrode system (mild steel samples entrenched in a Teflon holder exposed to 1 square cm corrosive medium; a saturated Hg_2Cl_2 electrode and platinum plate are considered as the working, reference, and counter electrodes) and an electrochemical cell in 3.5% NaCl solution (maintaining pH 7.5 at 32 °C). The 3.5% NaCl solutions closely resembled seawater characteristics, wherein many produced steel parts (in particular, those used in marine applications) undergo corrosion and therefore many studies use 3.5% NaCl solution as the corrosive medium for testing [68–70]. In 3.5% NaCl solution, by upholding pH neutral of corrosive medium, the coated samples are dipped and the attainment of the steady-state potential of the solution medium is ensured before measurements. Potentiodynamic polarization plots are drawn by considering the varied potentials ranges of ±200 mV and scanned rate of 0.01 V/s correspond to open circuit potential. EIS data was acquired with the help of open circuit potential at wide

frequency distribution ranges of 10 mHz to 100 kHz. ZSimpWin 3.21 software platform was utilized to draw the Nyquist plots based on collected impedance data. Figure 2 describes the characterization and testing of electrodeposited coatings discussed in detail in the authors' earlier studies. [44,63].

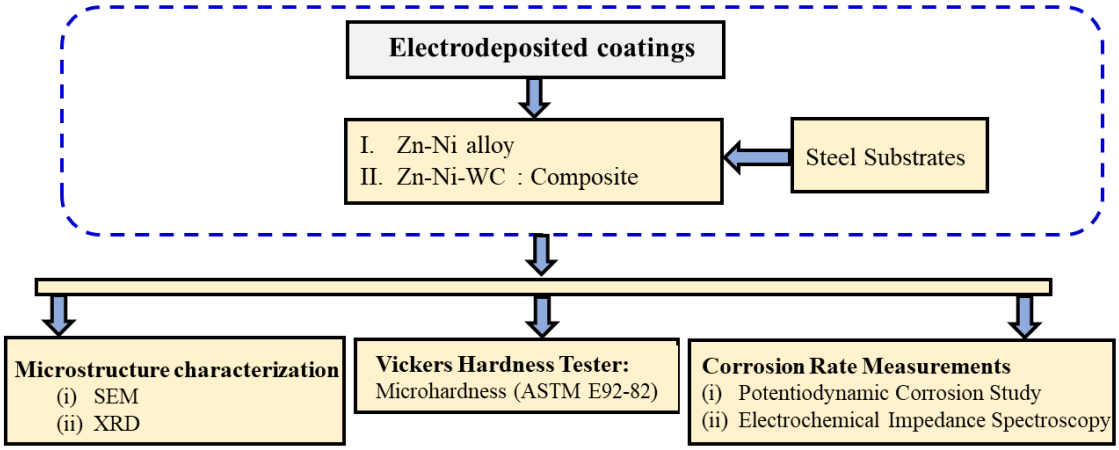

Figure 2. Flowchart of characterization and testing of electrodeposited coatings.

3. Results

This section describes the results of characterization (XRD and SEM) of Zn–Ni and WC particles. Furthermore, the Ni and WC nanoparticles' impact on the electrodeposition of Zn was analyzed with cathodic polarization curves, cyclic voltammogram studies, and texture coefficients. Furthermore, the electrodeposited Zn–Ni alloy and the Zn–Ni–WC composite nanocoatings are subjected to microhardness tests and the characterization of the corrosion rates.

3.1. Tungsten Carbide (WC) Particle Characterization

XRD pattern and SEM morphologies of WC particles (supplied by Himedia Laboratories Pvt. Ltd., Bangalore, India) are presented in Figure 3. XRD patterns of as-received WC powder show only the presence of single-phase peaks of WC particles (refer to Figure 3a). The peak intensity of the XRD patterns is matched with JCPDS file card number 59-0939. The WC particle morphologies were also examined via SEM. The average crystallite size of the WC particles was measured after considering at least 50 powder particles for measurement. The median crystallite size of the WC particles is computed according to Sherrer's model and is found to be equal to 97 nm. The SEM morphology displayed the presence of nano-sized particles agglomerated with fine and spherical-shaped WC particles (refer to Figure 3b).

3.2. Electrodeposition

The cathodic polarization and cyclic voltammetric experiments were used to analyze the effect of WC particles on the electrodeposition of the Zn–Ni alloy. The bath solution was polarized cathodically with and without the presence of WC particles (concentration of 1.0 g/L). In Figure 4a, curve (a) represents the polarization of the Zn–Ni alloy deposition from the bath solvent without WC particles. Curve (b) represents the polarization of the Zn–Ni–WC composite deposition obtained from a bath solvent comprising of an evenly distributed 1.0 g/L concentration of WC particles. For scanning, the range of potential was kept fixed equal to 0 to −1.6 V (Figure 4a). The WC particle inclusion in the electrolyte caused a reduction in Zn–Ni potential, which causes the curve (b) to shift slightly towards the negative side [71]. This occurs due to a greater reduction in the active sites on the cathode as a result of reduced current density. The inorganic nature of the WC particles causes a reduction in ionic diffusion. It is important to note that the electrochemical

reactants are unaffected by these processes. The WC particle incorporation on the cathode site prevents Zn–Ni accumulation and reduces the grain size of composite coating (Zn–Ni–WC). Similar observations are seen in the composite (Zn–Ni–Fe_2O_3 and Zn–Ni–CO) coatings [44,46]. This negative potential shift corresponds to a bath solution containing a 1 g/L concentration of WC particles that are much more pronounced than the Zn–Ni alloy. This shift is due to the presence of WC particles in bath solution which increases the cathodic surface area, and its adsorption to the Zn–Ni alloy. Similar observations are reported with carbon nanotube (CNT) particles electrodeposited on Zn [68].

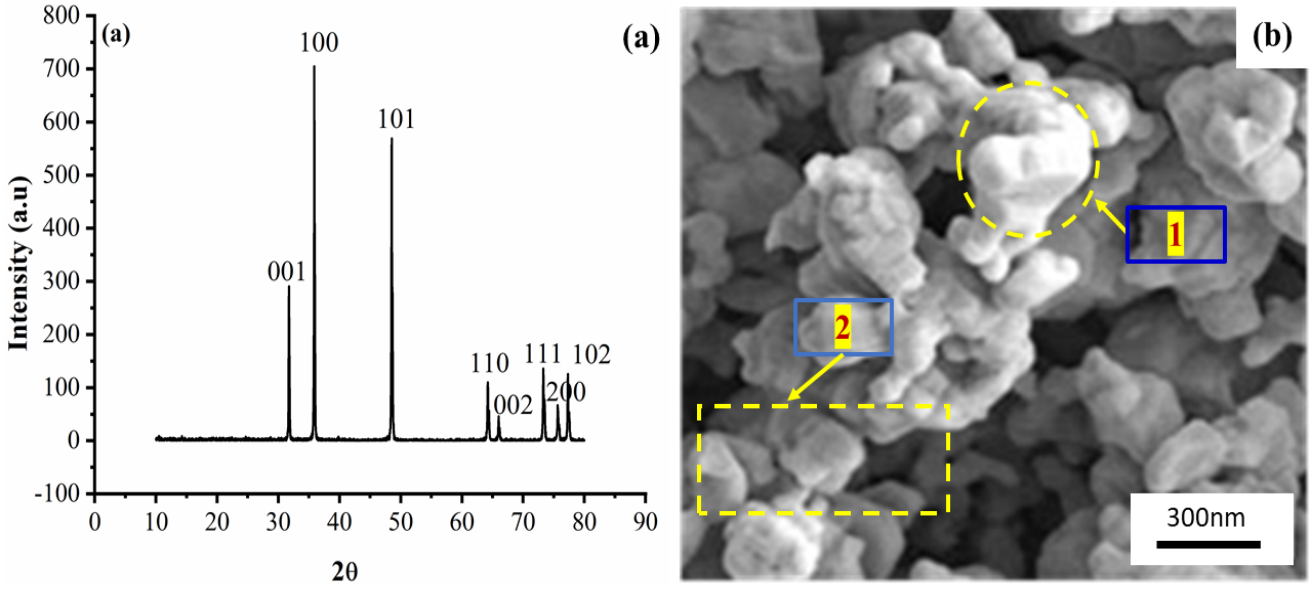

Figure 3. (**a**) XRD pattern and (**b**) SEM image of WC Particle (1 reveals fine and spherical morphology and 2 reveals agglomeration).

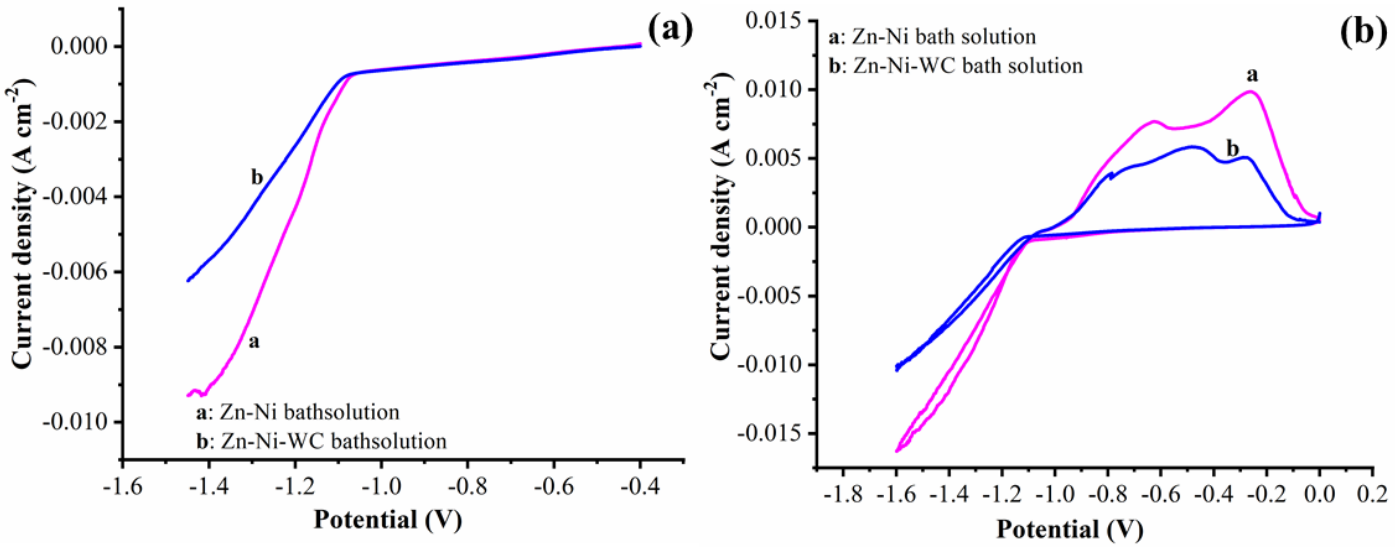

Figure 4. Zn–Ni alloy and Zn–Ni–WC composites result showing (**a**) Cathodic PC (**b**) Cyclic Voltammograms.

The cyclic voltammograms were recorded corresponding to the Zn–Ni alloy and Zn–Ni–WC composites bath solutions (refer to Figure 4b). The cyclic voltammetry analysis was conducted subjected to a scanning potential ranging from 0.2 to −1.8 V and then switched back to +0.2 V at a 100 mV/s scan rate (refer to Figure 4b). From Figure 4b, curve (a) represents the cyclic voltammograms corresponding to the Zn–Ni bath solution, and

curve (b) corresponds to the Zn–Ni composite bath solutions with 1 g/L of the nano-sized WC particles. In the forward scan, there was a reduction of Zn–Ni and WC was observed, which depicts the particle deposition on the cathode electrode surface. In Figure 4b, it was observed that the potential from 0 to −1.1 V showed no changes in the current which demonstrate no reactions seen on the cathode electrode surface. Towards more negative potential from −1.1 to −1.6 V, the current tends to decrease rapidly with reduced Zn–Ni and tungsten carbides on the cathode electrode surface. In the reverse scan, the crossover tends to be seen at −1.1 V where there will be the initiation of oxidation in the Zn–Ni and Zn–Ni–WC from the cathode electrode surface. The decrease in current density for the Zn–Ni–WC indicates that there will be difficulty in the dissolution rate of the Zn–Ni–WC composite compared to the Zn–Ni alloy. The curves also contribute to the following explanations.

In the anodic portion of the cyclic voltammograms, the anodic peak current was decreased for the Zn–Ni–WC composites compared to the Zn–Ni alloy coating (i.e., curve a < curve b). This indicates the effect of WC particles on the dissolution of the Zn–Ni coating. This could be attributed to the enhanced resistance to corrosion with the composite coating compared to the Zn–Ni alloy deposits. The addition of WC to the Zn–Ni alloy appreciably improved the corrosion resistance. The metal surface possessing defects (such as flaws, caverns, and grooves) higher than micrometers in size is filled effectively with the WC nanoparticles. Note that during the corrosion phenomenon, the presence of micro-gaps act as binding sites for metal solvation. Typically, such gaps are filled by WC particles that ensure a pore-free composite film, which results in a lower corrosion rate [68,69]. In the cathodic region, the Zn–Ni composite curve transferred towards higher negative potential than the Zn–Ni alloy bath solution, which suggests a greater possible grain size reduction in the Zn–Ni composites containing 1 g/L of WC particles. The findings are consistent with previous research on Ni–SiC alloy coatings [70].

3.3. Characterization of the Deposits

The XRD patterns that correspond to the Zn–Ni deposits, with and without WC nanoparticles (1 g/L concentration), are shown in Figure 5, wherein the peak intensity is matched to JCPD file card number 03-065-1252. Figure 5b of XRD graphs displays the decreased intensity peaks of diffraction lines of <510>, <−513> compared to the Zn–Ni alloy coatings. The XRD intensities of samples are compared after consulting the procedure employed in the previously published literature [44,63,68,71–74].

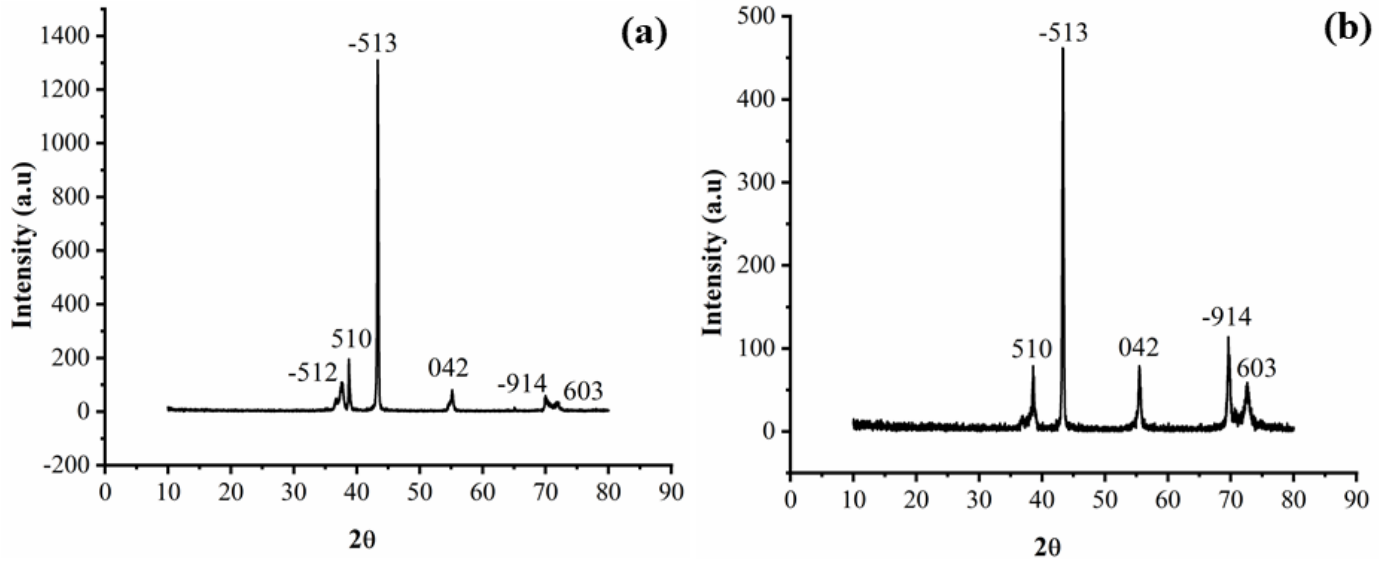

Figure 5. XRD pattern: (**a**) Zn–Ni alloy and (**b**) Zn–Ni–WC composites nanocoating.

The Scherrer equation was applied to determine the average crystallite size of electrodeposits, i.e., Zn–Ni alloy and Zn–Ni–WC composite coatings were found equal to 91 nm and 83 nm, respectively. A greater reduction in the average crystallite size of the composites coating was observed than Zn–Ni alloy coating. The WC nanoparticle inhibits the crystal growth of Zn–Ni alloy by offering a larger surface area for fresh nucleation. Furthermore, the WC nanoparticles' inclusion in metal deposits may offer changes in the metallic coating crystal structure, which results in reduced crystallite size in composites coatings. During the electrodeposition technique, the WC particles act as a protuberance in the metal electrode interface, which causes increased current density and nucleation rate, which results in reduced grain size by impeding crystal growth in the electrodeposits [72,73].

The texture coefficient studies were conducted to determine the preferred orientation of crystallite in the electrodeposit. The texture coefficient (Figure 6) was calculated for each peak of diffraction patterns. The Texture coefficient calculations were made by applying Be'rube' and L'Esperance, which is explained in detail in previous work [44,74]. From the T_C calculation, the Zn–Ni alloy coatings exhibited a maximum orientation in the <330> plane corresponding to minimum surface energy. The inclusion of the WC nanoparticles did not change the preferred orientation of the zinc–nickel matrix. Both the chosen orientations possess the highest Tc value, implying that the zinc–nickel deposition in that plane has the maximum proportion of crystallographic orientations. The above findings show that the inclusion of WC particles in the bath solution and matrix has a strong effect on the morphology of the electrodepositing coating and preferred orientation. Shi et al.'s findings with Ni–Co–CNTs coatings are in good agreement with the observed results [75].

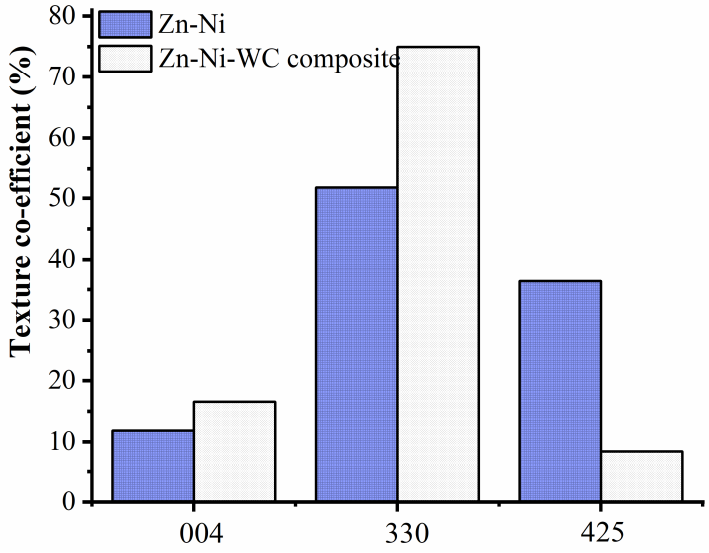

Figure 6. Texture coefficient (Tc) of Zn–Ni alloy and Zn–Ni–WC composites nanocoating.

The surface morphologies of Zn–Ni alloy and Zn–Ni–WC composites coatings are subjected to SEM are shown in Figure 7. Figure 7a shows the presence of excessive accumulation of Zn–Ni platelets at random in the Zn–Ni alloy coatings. However, in the Zn–Ni–WC composites, the Zn–Ni platelets are well stacked on the steel substrate. In addition, the deposition of the Zn–Ni coating was uneven and coarse, whereas the deposition of the Zn–Ni–WC composite nanocoating had a smooth and fine-grained structure as can be seen in the SEM images in Figure 7a,b. The WC nanoparticles embedded in the Zn–Ni matrix provide more opportunity for the reduction of Zn–Ni ions and limit the crystal growth of Zn–Ni ions over the WC particles. This led to the formation of reduced crystallite size in composites. Figure 7b shows the refined grain structure, which probably occurred because the WC nanoparticles initiated more nucleation sites at distinct locations that limit crystal growth. Similar observations are found with the addition of CNT particles

in nanocomposite coatings [68,69,75]. Furthermore, it was found that the WC particles refined the structure of the the Zn–Fe matrix in the Zn–2Fe–WC composite [54].

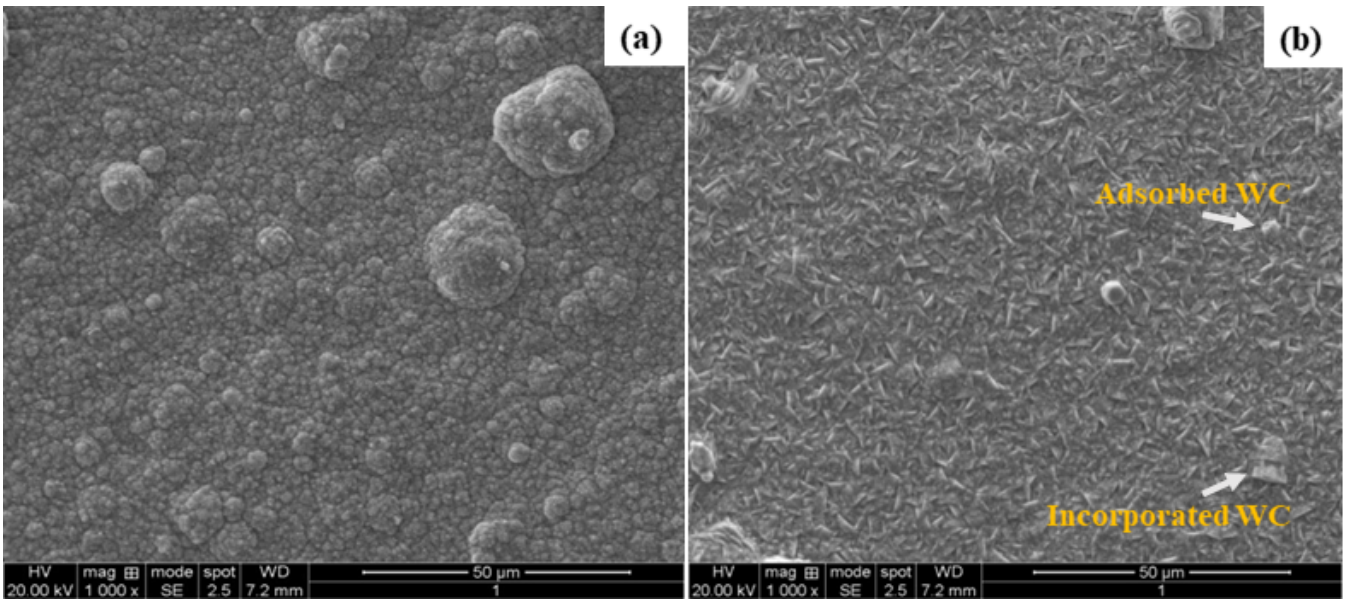

Figure 7. SEM morphology of coatings: (**a**) Zn–Ni alloy and (**b**) Zn–Ni–WC composites.

The presence of WC nanoparticles was also observed on the surface of the deposit. The WC nanoparticles function as a potential barrier that protects the electrodeposits from corrosion by minimizing the local defects (flaws, gaps, grooves) on the coated surface. The WC nanoparticles fill such gaps and ensure pore-free composite film, which often enhances the corrosion resistance in Zn–Ni–WC composite coatings. Similar observations are seen with the presence of Fe_2O_3, CNT, and Co nanoparticles in Zn–Ni-based composite coatings [44,46,68]. EDAX pattern corresponds to Zn–Ni alloy and Zn–Ni–WC composites nanocoating deposits are presented in Figure 8. The presence of Ni in the alloy (refer to Figure 8a) and elements such as W and C in the composite electrodeposits (refer to Figure 8b) indicate that WC particles were successfully incorporated into the Zn–Ni matrix.

The microhardness of nanocoating corresponds to Zn–Ni alloy and the Zn–Ni–WC composite of electrodeposits is presented in Figure 9. The average values of microhardness of the Zn–Ni alloy and the Zn–Ni–WC composite coatings are found to be equal to 97 $\pm$ 0.4 HV and 105.3 $\pm$ 0.5 HV, respectively. The Zn–Ni–WC composite nanocoating offered higher hardness than that of the Zn–Ni alloy coating (refer to Figure 9). The higher microhardness of the Zn–Ni–WC composite nanocoating is attributed to the uniform dispersal of WC particles, which might have strengthened or hardened the composites. Similar observations were found in WC–Bronze–Ni–Mn diamond-based composites and WC-reinforced Ni60 composite coatings [76,77]. During the hardness testing, scattered WC particles in the fine-grained matrix may hinder dislocation movements and restrain the plastic flow. The resulting composite coatings offered higher deformation. The microhardness corresponds to electrodeposited Zn [51], Zn–WO_3 [51], Zn–Ni alloy, and Zn–Ni–WC composite nanocoatings were found to be equal to 47.6 HV, 73.2 HV, 97 HV, and 105.3 HV, respectively. Compared to WO_3 nanoparticles metallic, Ni and WC particles improved the microhardness to a greater extent on the coatings. Note that the addition of Ni metallic particles to pure Zn, i.e., Zn–Ni alloy, enhanced microhardness by 103.78% compared to pure Zn. The addition of WC particles to Zn–Ni alloy, i.e., Zn–Ni–WC composites, resulted in an 8.56% increased microhardness in the Zn–Ni alloy. Higher hardness of the Zn–Ni–WC composites are attributed to the following [78]: Zn possesses better wettable characteristics, wherein the nanoparticles (WC and Ni) are electrodeposited with Zn matrix on a steel substrate where nickel particles grow progressively on WC particles, which cover

the local defects (gaps or pores) between the grains and ensure new nucleation sites on the coating surface, resulting in grain refinement (Hall–Petch relationship); dispersion strengthening (Orowan mechanism); and expanding the grain boundaries with reduced dislocation movement causes increased microhardness.

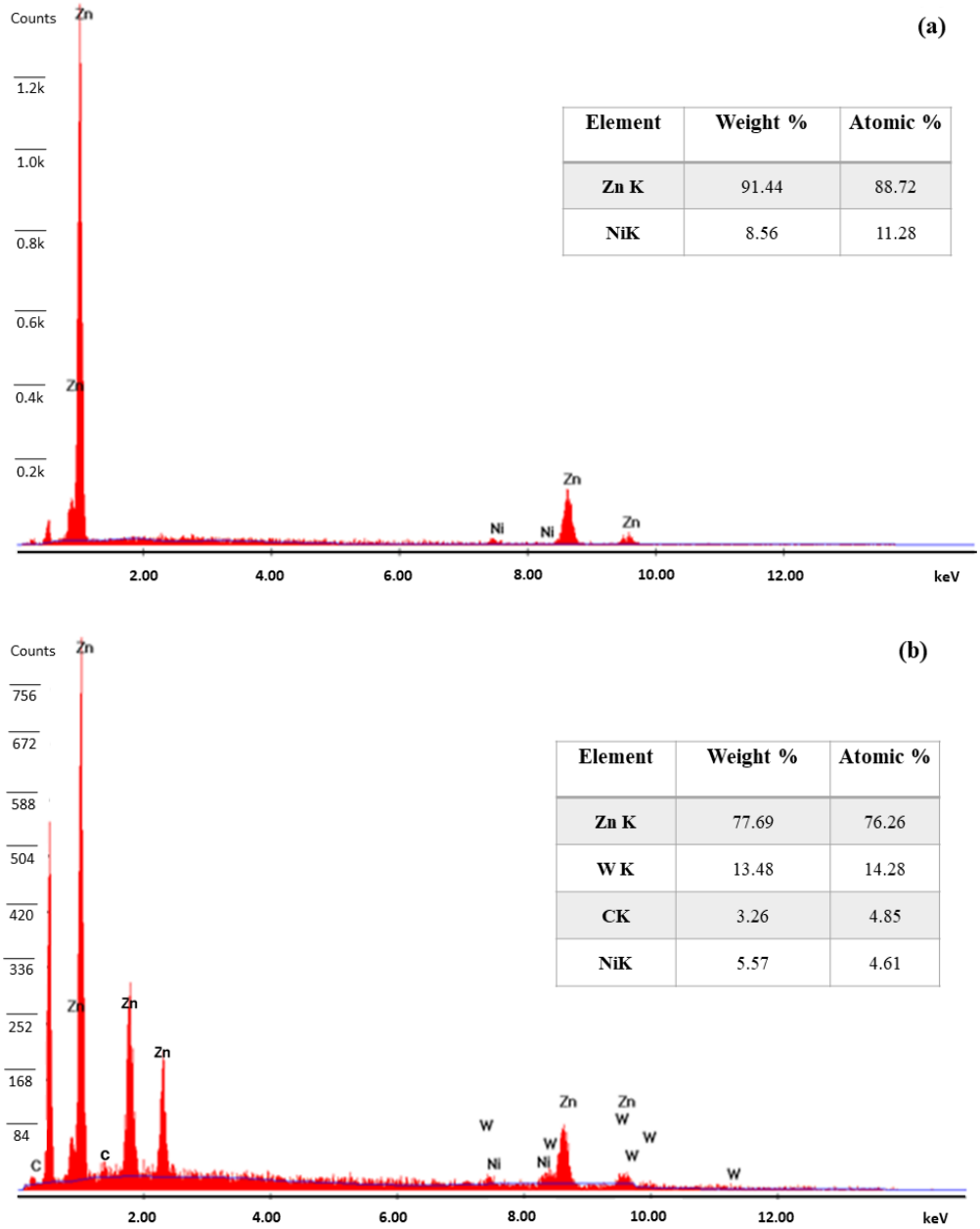

Element	Weight %	Atomic %
Zn K	91.44	88.72
NiK	8.56	11.28

Element	Weight %	Atomic %
Zn K	77.69	76.26
W K	13.48	14.28
CK	3.26	4.85
NiK	5.57	4.61

Figure 8. EDAX Patterns of coatings: (**a**) Zn–Ni alloy and (**b**) Zn–Ni–WC composites.

3.4. Corrosion Behavior of the Electrodeposited Coatings

Figure 10a presents the potentiodynamic curves correspond to Zn–Ni alloy and Zn–Ni–WC composites coating recorded after 5 min of dwell time of samples exposed to 3.5% NaCl corrosive media. Table 2 presents the details of corrosion kinetic parameters and appropriate understanding could help to predict corrosion behavior. Note that the potentiodynamic curve method is widely accepted in industrial and research laboratory practices to estimate the corrosion rate. However, potentiodynamic curves give large information on electrochemical kinetic parameters and could damage the specimen surfaces while measuring the presence of large potential disturbances [79,80]. Figure 10b shows the Zn–Ni–WC composites nanocoating resulted with lower negative potential and lesser

current densities than the Zn–Ni alloy. Thereby, the Zn–Ni–WC composite nanocoating has better corrosion resistance than the Zn–Ni alloy. The research findings are in good agreement with published literature [41]. Figure 10b illustrates the anodic polarization characteristics of the coatings. The curves with better correlation demonstrate that the WC particles do not have a significant effect on the dissolution process. However, the curve differentiates at the lesser negative potential in contrast to the potential of the Zn–Ni alloy dissolution process. Note that the potential of the Zn–Ni–WC composite coating resulted with slightly less negative or positive than Zn–Ni alloy corresponds to current density values. The Zn–Ni–WC composite nanocoating exhibited a slightly better and noble character than Zn–Ni alloy, revealed from anodic polarization.

The electrochemical method uses an electrode/solution interface in corrosive media to record the EIS data (Figure 10c). The Zn–Ni alloy and Zn–Ni–WC composite coatings electrochemical impedances were measured with the help of open circuit potential (OCP) correspond to frequency ranges of 100 kHz to 0.1 mHz. Nyquist plots were recorded in a 3.5% NaCl solution that could help to display the EIS data. The Nyquist plots (curves were fitted using Zsimpwin 3.2 software) acquired are inserted with the analogous circuit correspond to Zn–Ni alloy and Zn–Ni–WC composite electrodeposit coating is shown in Figure 11. Table 3 shows the electrochemical parameters derived from the fitted curves. A semi-circle of the Zn–Ni composite containing a 1.0 g/L concentration of WC particles has a larger diameter than the Zn–Ni alloy deposit, as shown in Figure 10c. Figure 10c, curve b of Zn–Ni–WC composites showed higher corrosion resistance than Zn–Ni alloy deposits. The obtained results were analogous to the published literature [42,43].

Table 2. Electrochemical parameters of the coatings derived from potentiodynamic plots.

Samples	βa (V^{-1})	β_c (V^{-1})	E_{rror} (V)	i_{corr} (A)	Corrosion Rate (Å/min)
Zn–Ni	27.531	4.914	−1.027	4.180×10^{-6}	1.192
Zn–Ni–WC coating	23.994	3.759	−1.007	2.437×10^{-6}	0.6948

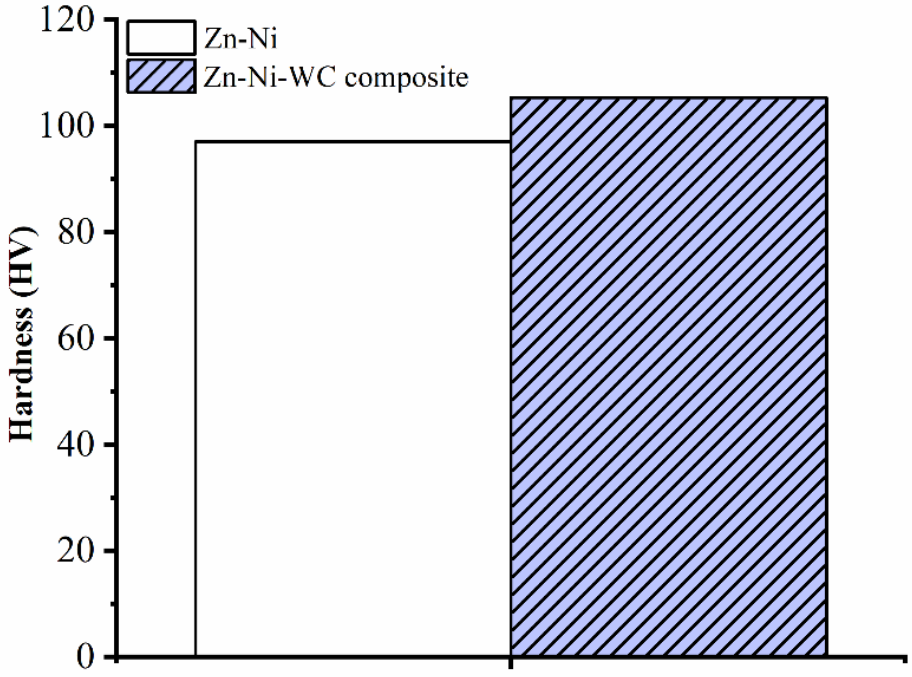

Figure 9. Vicker's microhardness for electrodeposited coatings (Zn–Ni alloy and Zn–Ni–WC composites).

The corrosion rate of Zn [51], Zn–WO_3 [51], Zn–Ni alloy, and Zn–Ni–WC composites are found equal to 32.69, 2.803, 1.192, and 0.6948 Å/min, respectively. Compared to WO_3 nanoparticles, Ni metallic ions alloyed with the Zn matrix exhibited a 57.47% decreased corrosion rate in coatings [51]. It is important to note that the addition of WC nanoparticles to Zn–Ni alloy, i.e., Zn–Ni–WC composites, resulted in a 41.71% decreased corrosion rate compared to the Zn–Ni alloy. This demonstrates that Zn–Ni–WC composites-based passive films protect the steel substrate effectively from electrochemical deterioration when subjected to corrosive media.

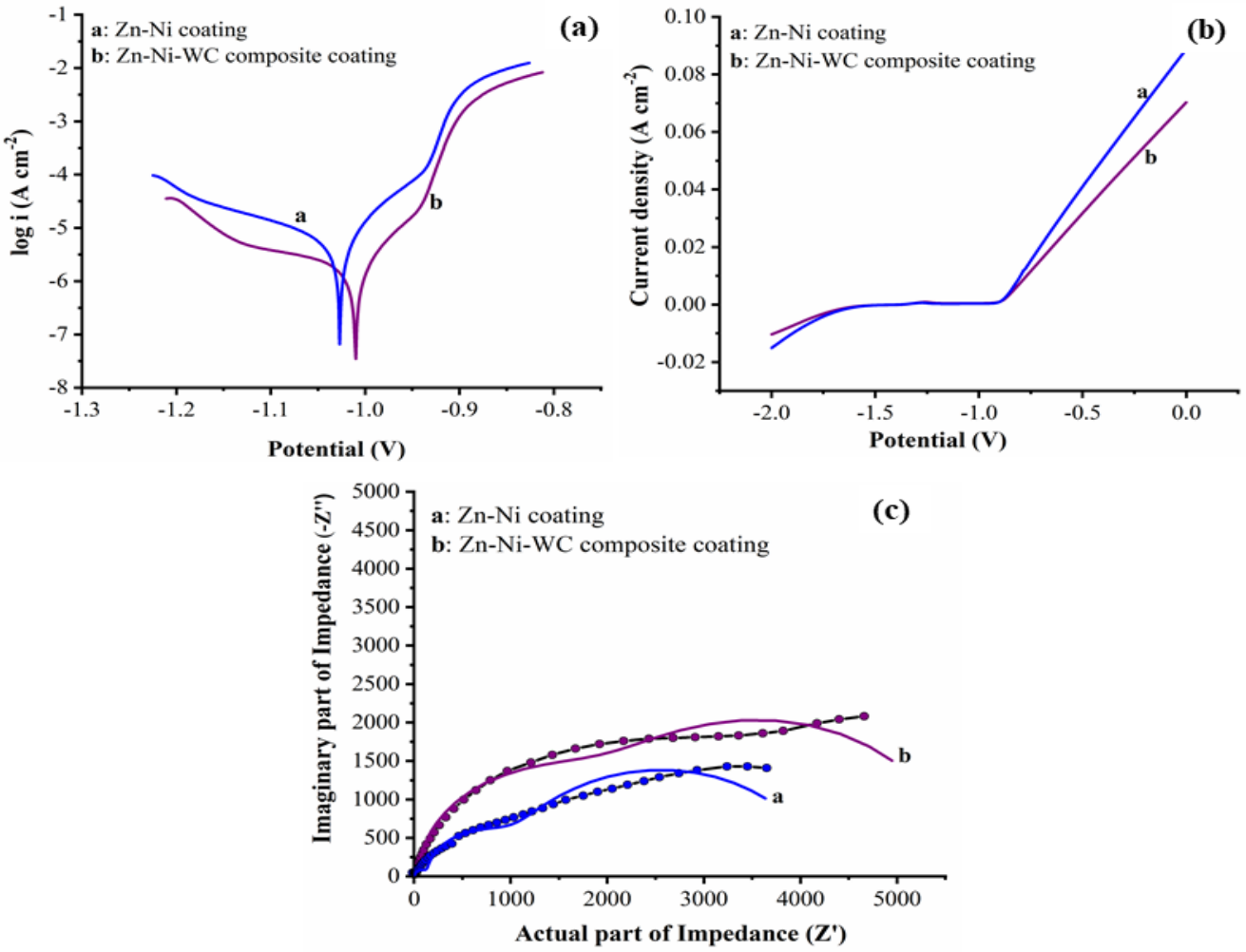

Figure 10. Zn–Ni alloy and Zn–Ni–WC composites showing (**a**) potentiodynamic curves of the coatings (**b**) anodic PC of coatings (**c**) impedance spectra.

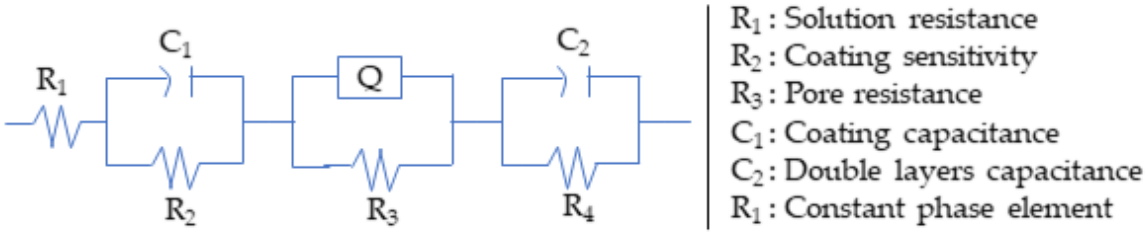

Figure 11. Circuit for Zn–Ni alloy and Zn–Ni–WC composite electrodeposits.

Table 3. Electrochemical kinetic parameters of the coatings extrapolated from EIS.

Samples	R_1 $\Omega \cdot cm^2$	R_2 $\Omega \cdot cm^2$	C_1 (F)	R_3 $\Omega \cdot cm^2$	Q	R_4 $\Omega \cdot cm^2$	C_2 (F)	Rp $\Omega \cdot cm^2$
Zn–Ni	3.88×10^{-8}	128.1	2.08×10^{-7}	3332	2.163×10^{-5}	806.9	2.138×10^{-6}	4267.0
Zn–Ni–WC coating	23.994	3.759	−1.007	2.437×10^{-6}	0.6948	47.45	9.546×10^{-7}	5621.4

4. Conclusions

The electrochemical deterioration of steel parts due to corrosion can result in huge production, economic, and environmental losses. In this work, electrodeposited coatings (Zn–Ni and Zn–Ni–WC) were prepared in an environmentally friendly bath solution. These coatings were then treated in a cost-effective method and applied on a steel substrate. The potential benefits of Zn, Ni, and WC in terms of biocompatibility and properties were used to prepare the Zn–Ni alloys and the Zn–Ni–WC composite nanocoatings. The impact of the Ni metallic particles and the WC nanoparticles on electrodeposited Zn was evaluated for microhardness and corrosion rate of electrodeposited coatings. The following conclusions were drawn:

1. On mild steel specimens, Zn–Ni alloy and Zn–Ni–WC coatings were successfully developed, which can be used in industrial applications to protect parts from chemical/electrochemical deterioration.
2. The incorporation of WC particles into the Zn–Ni matrix was confirmed from the SEM and EDAX spectroscopy.
3. The composite coating's SEM images show a smoother grained deposit than the Zn–Ni alloy coating.
4. The XRD results shows that the composite coating has smaller crystallites than the Zn–Ni coating.
5. The hardness test revealed that the Zn–Ni–WC composite coating has a higher hardness compared to the Zn–Ni coating. The addition of Ni metallic particles to pure Zn, i.e., Zn–Ni alloy, enhanced microhardness by 103.78% compared to pure Zn. The addition of WC particles to the Zn–Ni alloy i.e., Zn–Ni–WC composites, resulted in 8.56% increased microhardness in the Zn–Ni alloy.
6. Polarization, potentiodynamic curves, and impedance spectra techniques were used to investigate the improved corrosion rate of the Zn–Ni–WC composite coating. Ni metallic ions alloyed with the Zn matrix exhibited a 57.47% decreased corrosion rate in coatings compared to WO_3 particles. The addition of WC nanoparticles to Zn–Ni alloy, i.e., Zn–Ni–WC composites, resulted in a 41.71% decreased corrosion rate than the Zn–Ni alloy.
7. Zn–Ni–WC composite nanocoatings could protect the steel surface effectively from electrochemical deterioration subjected to corrosive media.

Author Contributions: Conceptualization, C.M.P.K., A.L. and M.P.G.C.; methodology, C.M.P.K. and M.P.G.C.; software, C.M.P.K. and M.P.G.C.; validation, A.L., K.G. and D.Y.P.; formal analysis, C.M.P.K., A.L., K.G. and D.Y.P.; investigation, C.M.P.K.; resources, M.P.G.C., K.G. and D.Y.P.; writing—original draft preparation, C.M.P.K. and M.P.G.C.; writing—review and editing, M.P.G.C., K.G., A.L. and D.Y.P. All authors have read and agreed to the published version of the manuscript.

Funding: This research received no external funding.

Institutional Review Board Statement: Not applicable.

Informed Consent Statement: Not applicable.

Data Availability Statement: Data can be made available upon request.

Conflicts of Interest: The authors declare no conflict of interest.

References

1. Bajaj, P.; Hariharan, A.; Kini, A.; Kürnsteiner, P.; Raabe, D.; Jägle, E.A. Steels in additive manufacturing: A review of their microstructure and properties. *Mater. Sci. Eng. A* **2020**, *772*, 138633. [CrossRef]
2. Qudeiri, J.E.A.; Zaiout, A.; Mourad, A.H.I.; Abidi, M.H.; Elkaseer, A. Principles and characteristics of different EDM processes in machining tool and die steels. *Appl. Sci.* **2020**, *10*, 2082. [CrossRef]
3. Wei, H.; Chen, Y.L.; Yu, W.; Su, L.; Wang, X.; Tang, D. Study on corrosion resistance of high-strength medium-carbon spring steel and its hydrogen-induced delayed fracture. *Constr. Build. Mater.* **2020**, *239*, 117815. [CrossRef]
4. Sumita, M.; Hanawa, T.; Teoh, S.H. Development of nitrogen-containing nickel-free austenitic stainless steels for metallic biomaterials. *Mater. Sci. Eng. C* **2004**, *24*, 753–760. [CrossRef]
5. Keerthana, A.K.; Ashraf, P.M. Carbon nanodots synthesized from chitosan and its application as a corrosion inhibitor in boat-building carbon steel BIS2062. *Appl. Nanosci.* **2020**, *10*, 1061–1071. [CrossRef]
6. Di Schino, A. Manufacturing and Applications of Stainless Steels. *Metals* **2020**, *10*, 327. [CrossRef]
7. Chen, Y.; Yang, B.; Zhou, Y.; Wu, Y.; Zhu, H. Evaluation of pitting corrosion in duplex stainless steel Fe20Cr9Ni for nuclear power application. *Acta Mater.* **2020**, *197*, 172–183. [CrossRef]
8. Schmitt, G. *Global Needs for Knowledge Dissemination, Research, and Development in Materials Deterioration and Corrosion Control*; World Corrosion Organization: New York, NY, USA, 2009.
9. The World Corrosion Organization. Available online: https://corrosion.org/ (accessed on 2 June 2021).
10. Zotov, S.V. Analysis of galvanized coatings applied on general purpose wire. In *Solid State Phenomena*; Trans Tech Publications Ltd.: Bäch, Switzerland, 2020; Volume 299, pp. 827–832. [CrossRef]
11. Hegyi, A.; Dico, C.; Constantinescu, H.; Baera, C. Influence of hot-dip galvanizing of reinforcement on the kinetics and thermodynamics of corrosion process in concrete. *Procedia Eng.* **2017**, *181*, 226–233. [CrossRef]
12. Song, P.; Liu, M.; Jiang, X.; Feng, Y.; Wu, J.; Zhang, G.; Wang, D.; Dong, J.; Chen, X.; Lou, L. Influence of alloying elements on hot corrosion resistance of nickel-based single crystal superalloys coated with Na_2SO_4 salt at 900 °C. *Mater. Des.* **2021**, *197*, 109197. [CrossRef]
13. Nady, H.; El-Rabiei, M.M.; Samy, M.; Badawy, W.A. The Influence of Alloying El-ements (Al, Ni and Zn) on the Corrosion Resistance of Some Cu-Ternary Alloys in Na2SO4 Solutions. *J. Biol. Tribocorros.* **2020**, *6*, 1–13. [CrossRef]
14. Wang, Y.Q.; Han, J.; Wu, H.C.; Yang, B.; Wang, X.T. Effect of sigma phase precipitation on the mechanical and wear properties of Z3CN20. 09M cast duplex stainless steel. *Nucl. Eng. Des.* **2013**, *259*, 1–7. [CrossRef]
15. Baruwa, A.D.; Akinlabi, E.T.; Oladijo, O.P. Surface coating processes: From conventional to the advanced methods: A short review. In *Advances in Manufacturing Engineering, Lecture Notes in Mechanical Engineering*; Emamian, S.S., Awang, M., Yusof, F., Eds.; Spring: Berlin/Heidelberg, Germany, 2020.
16. Koga, G.Y.; Wolf, W.; Schulz, R.; Savoie, S.; Bolfarini, C.; Kiminami, C.S.; Botta, W.J. Corrosion and wear properties of FeCrMnCoSi HVOF coatings. *Surf. Coat. Technol.* **2019**, *357*, 993–1003. [CrossRef]
17. Gu, Y.; Xia, K.; Wu, D.; Mou, J.; Zheng, S. Technical characteristics and wear-resistant mechanism of nano coatings: A review. *Coatings* **2020**, *10*, 233. [CrossRef]
18. Chalker, P.R.; Bull, S.J.; Rickerby, D.S. A review of the methods for the evaluation of coating-substrate adhesion. *Mater. Sci. Eng. A* **1991**, *140*, 583–592. [CrossRef]
19. Schrooten, J.; Helsen, J.A. Adhesion of bioactive glass coating to Ti_6Al_4V oral implant. *Biomaterials* **2000**, *21*, 1461–1469. [CrossRef]
20. Fotovvati, B.; Namdari, N.; Dehghanghadikolaei, A. On coating techniques for surface protection: A review. *J. Manuf. Mater. Process.* **2019**, *3*, 28. [CrossRef]
21. Arango, S.; Peláez-Vargas, A.; García, C. Coating and surface treatments on orthodontic metallic materials. *Coatings* **2013**, *3*, 1–15. [CrossRef]
22. Darband, G.B.; Aliofkhazraei, M.; Khorsand, S.; Sokhanvar, S.; Kaboli, A. Science and engineering of superhydrophobic surfaces: Review of corrosion resistance, chemical and mechanical stability. *Arab. J. Chem.* **2020**, *13*, 1763–1802. [CrossRef]
23. Chen, Z.; Hao, L.; Chen, A.; Song, Q.; Chen, C. A rapid one-step process for fabrication of superhydrophobic surface by electrodeposition method. *Electrochim. Acta* **2012**, *59*, 168–171. [CrossRef]
24. She, X.; Wu, J.; Xu, H.; Mo, Z.; Lian, J.; Song, Y.; Liu, L.; Du, D.; Li, H. Enhancing charge density and steering charge unidirectional flow in 2D non-metallic semiconductor-CNTs-metal coupled photocatalyst for solar energy conversion. *Appl. Catal. B Environ.* **2017**, *202*, 112–117. [CrossRef]
25. Walsh, F.C.; Wang, S.; Zhou, N. The electrodeposition of composite coatings: Diversity, applications and challenges. *Curr. Opin. Electrochem.* **2020**, *20*, 8–19. [CrossRef]
26. Zhang, H.; Liu, Q.; Liu, T.; Zhang, B. The preservation damage of hydrophobic polymer coating materials in conservation of stone relics. *Prog. Org. Coat.* **2013**, *76*, 1127–1134. [CrossRef]
27. Chanana, M.; Liz-Marzán, L.M. Coating matters: The influence of coating materials on the optical properties of gold nanoparticles. *Nanophotonics* **2012**, *1*, 199–220. [CrossRef]
28. DeMasi-Marcin, J.T.; Gupta, D.K. Protective coatings in the gas turbine engine. *Surf. Coat. Technol.* **1994**, *68*, 522. [CrossRef]
29. Vignesh, S.; Shanmugam, K.; Balasubramanian, V.; Sridhar, K. Identifying the optimal HVOF spray parameters to attain minimum porosity and maximum hardness in iron based amorphous metallic coatings. *Def. Technol.* **2017**, *13*, 101–110. [CrossRef]

30. Rajahram, S.S.; Harvey, T.J.; Wood, R.J.K. Erosion–corrosion resistance of engineering materials in various test conditions. *Wear* **2009**, *267*, 244–254. [CrossRef]
31. Chavan, N.M.; Kiran, B.; Jyothirmayi, A.; Phani, P.S.; Sundararajan, G. The corrosion behavior of cold sprayed zinc coatings on mild steel substrate. *J. Therm. Spray Technol.* **2013**, *22*, 463–470. [CrossRef]
32. Proskurkin, E.V.; Sukhomlin, D.A. A Study of the corrosion resistance of pump–compressor pipes with a diffusion zinc coating under the complicated conditions of gas-producing wells. *Prot. Met. Phys. Chem. Surf.* **2017**, *53*, 1288–1294. [CrossRef]
33. Roghanian, N.; Banthia, N. Development of a sustainable coating and repair material to prevent bio-corrosion in concrete sewer and waste-water pipes. *Cem. Concr. Compos.* **2019**, *100*, 99–107. [CrossRef]
34. Lee, L.; Behera, P.; Sriraman, K.R.; Chromik, R.R. The effect of contact stress on the sliding wear behaviour of Zn-Ni electrodeposited coatings. *Wear* **2018**, *400*, 82–92. [CrossRef]
35. Conde, A.; Arenas, M.A.; De Damborenea, J.J. Electrodeposition of Zn–Ni coatings as Cd replacement for corrosion protection of high strength steel. *Corros. Sci.* **2011**, *53*, 1489–1497. [CrossRef]
36. Sriraman, K.R.; Brahimi, S.; Szpunar, J.A.; Osborne, J.H.; Yue, S. Tribocorrosion behavior of Zn, Zn–Ni, Cd and Cd–Ti electrodeposited on low carbon steel substrates. *Surf. Coat. Technol.* **2013**, *224*, 126–137. [CrossRef]
37. El Hajjami, A.; Gigandet, M.P.; De Petris-Wery, M.; Catonne, J.C.; Duprat, J.J.; Thiery, L.; Raulin, F.; Pommier, N.; Starck, B.; Remy, P. Characterization of thin Zn–Ni alloy coatings electrodeposited on low carbon steel. *Appl. Surf. Sci.* **2007**, *254*, 480–489. [CrossRef]
38. Jiang, W.; Fan, Z.; Li, G.; Li, C. Effects of zinc coating on interfacial microstructures and mechanical properties of aluminum/steel bimetallic composites. *J. Alloys Compd.* **2016**, *678*, 249–257. [CrossRef]
39. Wang, S.; Zhou, B.; Zhang, X.; Sun, T.; Li, G.; Cui, J. Mechanical properties and interfacial microstructures of magnetic pulse welding joints with aluminum to zinc-coated steel. *Mater. Sci. Eng. A.* **2020**, *788*, 139425. [CrossRef]
40. Klekotka, M.; Zielińska, K.; Stankiewicz, A.; Kuciej, M. Tribological and anticorrosion performance of electroplated zinc based nanocomposite coatings. *Coatings* **2020**, *10*, 594. [CrossRef]
41. Malatji, N.; Popoola, A.P.I.; Fayomi, O.S.I. The effect of nanoparticulate loading on the fabrication and characterization of multi-doped Zn-Al_2O_3-Cr_2O_3 hybrid coatings on mild steel. *Int. J. Adv. Manuf. Tech.* **2017**, *90*, 2443–2452. [CrossRef]
42. Popoola, A.P.I.; Daniyan, A.A.; Umoru, L.E.; Fayomi, O.S.I. Effect of WO_3 nanoparticle loading on the microstructural, mechanical and corrosion resistance of Zn matrix/TiO_2-WO_3 nanocomposite coatings for marine application. *J. Mar. Sci. Technol.* **2017**, *16*, 102–109. [CrossRef]
43. Utu, I.D.; Muntean, R.; Mitelea, I. Corrosion and Wear Properties of Zn-Based Composite Coatings. *J. Mater. Eng. Perform.* **2020**, *29*, 5360–5365. [CrossRef]
44. PraveenKumar, C.M.; Venkatesha, T.V.; Vathsala, K.; Nayana, K.O. Electrodeposition and corrosion behavior of Zn–Ni and Zn–Ni–Fe_2O_3 coatings. *J. Coat. Technol. Res.* **2012**, *9*, 71–77. [CrossRef]
45. Lotfi, N.; Aliofkhazraei, M.; Rahmani, H.; Darband, G.B. Zinc–nickel alloy electrodeposition: Characterization, properties, multilayers and composites. *Prot. Met. Phys. Chem. S* **2018**, *54*, 1102–1140. [CrossRef]
46. Bhat, R.S.; Shet, V.B. Development and characterization of Zn–Ni, Zn–Co and Zn–Ni–Co coatings. *Surf. Eng.* **2020**, *36*, 429–437. [CrossRef]
47. Arrighi, C.; Savall, C.; Cohendoz, S.; Grosseau-Poussard, J.L.; Baissac, L.; Olivier, M.G.; Creus, J. Optimization of the morphology, structure and properties of high iron content Zn–Fe coatings by pulse electrodeposition. *Mater. Chem. Phys.* **2021**, *263*, 124366. [CrossRef]
48. Dini, J.W.; Johnson, H.R. *Electrodeposition of Zinc—Nickel Alloys Coatings*; (No. SAND-77–8511; CONF-771094–1); Sandia National Lab. (SNL-NM): Albuquerque, NM, USA, 1977.
49. Park, J.H.; Kosugi, D.; Hagio, T.; Kamimoto, Y.; Ichino, R.; Lee, M.H. Improvement in corrosion resistance of ternary Zn-Fe-Mo plating by additional Mo-oxide coating. *Surf. Coat. Technol.* **2020**, *389*, 125567. [CrossRef]
50. Toghan, A.; Abou-krisha, M.M.; Assaf, F.H.; El-Sheref, F. Effect of deposition potential on the mechanism and corrosion behavior of Zn-Fe-Co thin coatings electrochemically deposited on a steel substrate. *Int. J. Electrochem. Sci.* **2021**, *16*, 151044. [CrossRef]
51. Kumar, C.M.P.; Chandrashekarappa, M.P.G.; Kulkarni, R.M.; Pimenov, D.Y.; Giasin, K. The Effect of Zn and Zn–WO_3 Composites Nano-Coatings Deposition on Hardness and Corrosion Resistance in Steel Substrate. *Materials* **2021**, *14*, 2253. [CrossRef]
52. Miller, R.J.; Adeleye, A.S.; Page, H.M.; Kui, L.; Lenihan, H.S.; Keller, A.A. Nano and traditional copper and zinc antifouling coatings: Metal release and impact on marine sessile invertebrate communities. *J. Nanopart. Res.* **2020**, *22*, 547. [CrossRef]
53. Roventi, G.; Bellezze, T.; Fratesi, R. Electrodeposition of Zn–SiC nanocomposite coatings. *J. Appl. Electrochem.* **2013**, *43*, 839–846. [CrossRef]
54. Guan, Z.; Linsley, C.S.; Pan, S.; DeBenedetto, C.; Liu, J.; Wu, B.M.; Li, X. Highly Ductile Zn-2Fe-WC Nanocomposite as Biodegradable Material. *Metall. Mater. Trans. A* **2020**, *51*, 4406–4413. [CrossRef]
55. Blagoveshchenskiy, Y.V.; Isaeva, N.V.; Sinaiskiy, M.A.; Ankudinov, A.B.; Zelensky, V.A. Tuning the properties of refractory carbide nanopowders. *Org. Mater. Appl. Res.* **2018**, *9*, 924–929. [CrossRef]
56. Farahmand, P.; Liu, S.; Zhang, Z.; Kovacevic, R. Laser cladding assisted by induction heating of Ni–WC composite enhanced by nano-WC and La_2O_3. *Ceram. Int.* **2014**, *40*, 15421–15438. [CrossRef]
57. Paul, C.P.; Mishra, S.K.; Tiwari, P.; Kukreja, L.M. Solid-particle erosion behaviour of WC/Ni composite clad layers with different contents of WC particles. *Opt. Laser Technol.* **2013**, *50*, 155–162. [CrossRef]

58. Fernández, M.R.; García, A.; Cuetos, J.M.; González, R.; Noriega, A.; Cadenas, M. Effect of actual WC content on the reciprocating wear of a laser cladding NiCrBSi alloy reinforced with WC. *Wear* **2015**, *324*, 80–89. [CrossRef]
59. Pan, S.; Yao, G.; Sokoluk, M.; Guan, Z.; Li, X. Enhanced thermal stability in Cu-40 wt% Zn/WC nanocomposite. *Mater. Des.* **2019**, *180*, 107964. [CrossRef]
60. Guan, Z.; Linsley, C.S.; Hwang, I.; Yao, G.; Wu, B.M.; Li, X. Novel zinc/tungsten carbide nanocomposite as bioabsorbable implant. *Mater. Lett.* **2020**, *263*, 127282. [CrossRef]
61. He, L.; Liu, H.; Chen, D.; Chen, Z.; Bai, X. Fabrication of HAp/Ni biomedical coatings using an electro-codeposition technique. *Surf. Coat. Technol.* **2002**, *160*, 109–113. [CrossRef]
62. Ruthradevi, T.; Akbar, J.; Kumar, G.S.; Thamizhavel, A.; Kumar, G.A.; Vatsa, R.K.; Dannangoda, G.C.; Martirosyan, K.S.; Girija, E.K. Investigations on nickel ferrite embedded calcium phosphate nanoparticles for biomedical applications. *J. Alloys Compd.* **2017**, *695*, 3211–3219. [CrossRef]
63. Kumar, C.P.; Venkatesha, T.V.; Shabadi, R. Preparation and corrosion behavior of Ni and Ni–graphene composite coatings. *Mater. Res. Bull.* **2013**, *48*, 1477–1483. [CrossRef]
64. Mbugua, N.S.; Kang, M.; Zhu, J.; Liu, Y.; Zhang, Y.; Ndiithi, N.J. Synthesis and characterization of Ni–W/Cr2O3 nanocomposite coatings using electrochemical deposition technique. *Coatings* **2019**, *9*, 815. [CrossRef]
65. Sugiyama, S.; Ogawa, T.; He, L.; Wang, Z.; Adachi, Y. Quantitative analysis of the recovery process in pure iron using x-ray diffraction line profile analysis. *Materials* **2021**, *14*, 895. [CrossRef] [PubMed]
66. Lagos, K.J.; Marinkovic, B.A.; Debut, A.; Vizuete, K.; Guerrero, V.H.; Pardo, E.; Pontón, P.I. Towards iron-titanium oxide nanostructures from ecuadorian black mineral sands. *Minerals* **2021**, *11*, 122. [CrossRef]
67. Pardhasaradhy, N.V. *Practical Electroplating Hand Book*; Prentice Hall Inc Publications: Hoboken, NJ, USA, 1987.
68. Praveen, B.M.; Venkatesha, T.V. Electrodeposition and properties of Zn–Ni–CNT composite coatings. *J. Alloys Compd.* **2009**, *482*, 53–57. [CrossRef]
69. Chen, X.H.; Chen, C.S.; Xiao, H.N.; Cheng, F.Q.; Zhang, G.; Yi, G.J. Corrosion behavior of carbon nanotubes–Ni composite coating. *Surf. Coat. Technol.* **2005**, *191*, 351–356. [CrossRef]
70. Lee, H.K.; Lee, H.Y.; Jeon, J.M. Codeposition of micro- and nano-sized SiC Particles in the nickel matrix composite coatings obtained by electroplating. *Surf. Coat. Technol.* **2007**, *201*, 4711–4717. [CrossRef]
71. Fustes, J.; Gomes, A.; da Silva Pereira, M.I. Electrodeposition of Zn–TiO_2 nanocomposite films—effect of bath composition. *J. Solid State Electr.* **2008**, *12*, 1435–1443. [CrossRef]
72. Niu, Z.X.; Cao, F.H.; Wei, W.A.N.G.; Zhang, Z.; Zhang, J.Q.; Cao, C.N. Electrodeposition of Ni-SiC nanocomposite film. *Trans. Nonferr. Metals Soc. China* **2007**, *17*, 9–15. [CrossRef]
73. Deepa, K.; Venkatesha, T.; Nagaraja, C.; Vinutha, M. Electrochemical corrosion studies of Zn-CuO and Zn-NiO-CuO composite coatings on mild steel. *Anal. Bioanal. Electrochem.* **2017**, *9*, 374–389. Available online: https://www.sid.ir/en/journal/ViewPaper.aspx?id=660641 (accessed on 2 June 2021).
74. Mohankumar, P.C.; Venkatesha, V.T. Surfactants Effect on Zn–Si3N4 coating, electrochemical properties, and their corrosion behaviors. *Ind. Eng. Chem. Res.* **2013**, *52*, 12827–12837. [CrossRef]
75. Shi, L.; Sun, C.F.; Gao, P.; Zhou, F.; Liu, W.M. Electrodeposition and characterization of Ni–Co–carbon nanotubes composite coatings. *Surf. Coat. Technol.* **2006**, *200*, 4870–4875. [CrossRef]
76. Li, S.; Han, Z.; Meng, Q.; Zhao, X.; Cao, X.; Liu, B. Effect of WC nanoparticles on the microstructure and properties of WC-bronze-Ni-Mn based diamond composites. *Appl. Sci.* **2018**, *8*, 1501. [CrossRef]
77. Zhang, P.; Pang, Y.; Yu, M. Effects of WC particle types on the microstructures and properties of WC-reinforced Ni60 composite coatings produced by laser cladding. *Metals* **2019**, *9*, 583. [CrossRef]
78. Mohajeri, S.; Dolati, A.; Rezagholibeiki, S. Electrodeposition of Ni/WC nano composite in sulfate solution. *Mater. Chem. Phys.* **2011**, *129*, 746–750. [CrossRef]
79. Frankel, G.S. Electrochemical techniques in corrosion: Status, limitations, and needs. *J. Test. Eval.* **2014**, *42*, 517–538. [CrossRef]
80. Cai, S.Y.; Wen, L.; Jin, Y. A comparative study on corrosion kinetic parameter estimation methods for the early stage corrosion of Q345B steel in 3.5 wt% NaCl solution. *Int. J. Min. Met. Mater.* **2017**, *24*, 1112–1124. [CrossRef]